Biosensors and Bioelectronics 61 (2014) 209–214

Contents lists available at ScienceDirect

Biosensors and Bioelectronics

journal homepage: www.elsevier.com/locate/bios

Short communication

Highly sensitive and selective photoelectrochemical biosensor platform for polybrominated diphenyl ether detection using the quantum dots sensitized three-dimensional, macroporous ZnO nanosheet photoelectrode

Weili Li, Pengtao Sheng, Jin Cai, Hongyan Feng, Qingyun Cai *

State Key Lab of Chemo/Biosensing & Chemometrics, College of Chemistry & Chemical Engineering, Hunan University, Changsha 410082, China

ARTICLE INFO

Article history:
Received 16 February 2014
Received in revised form
5 April 2014
Accepted 23 April 2014
Available online 21 May 2014

Keywords:
Polybrominated diphenyl ether
Photoelectrochemical
Quantum dots
Immunosensor
Macroporous ZnO nanosheet

ABSTRACT

A novel photoelectrochemical (PEC) immunosensor for the rapid detection of 2,3′,4,5′,6-pentabromodiphenylether (BDE-121) was developed by coating a core–shell ZnS/CdTe/Mn–CdS/ZnS sensitized macroporous ZnO nanosheet (NS) photoelectrode with anti-BDE-121 polyclonal antibody. Here, core–shell CdTe/Mn–CdS quantum dots (QDs) benefit the signal amplification and photostability of the co-sensitized ZnO NS photoelectrode. After introducing the ZnS buffer layers between different interfaces (the ZnO NS and sensitizers; sensitizers and the electrolyte), the photoresponse was further enhanced. Under standard simulated illumination, the saturation photocurrent density of the co-sensitized photoelectrode is 6.23 mA cm^{-2}, the highest value reported to date for ZnO NS based photoelectrode. The BDE-121 was detected by monitoring the changes of the photocurrent signals of the immunosensor resulting from the immunoreaction. The immunosensor is sensitive, stable and highly specific toward BDE-121, displaying a linear range of 5 pM to 100 nM with a limit of detection of 3.98 pM. BDE-121 in paint samples was analyzed with the proposed sensor and gas chromatography–mass spectrometry (GC/MS), giving contents of 1.32 ± 0.02 ng mL^{-1} and 1.16 ng mL^{-1}, respectively.

1. Introduction

As important brominated flame retardants (BFRs), polybrominated diphenyl ethers (PBDEs) have effectively protected the safety of human lives and properties since 1970 s. There are three major commercial products: pentabromodip henylether (Penta-BDE) used in flexible polyurethane foam, octabromodiphenyl ether (Octa-BDE) used in acrylonitrile butadiene, and decabromodiphenyl ether (Deca-BDE) used in the high-impact polystyrene component of electronic equipments (Yang et al., 2013). The global production of PBDEs was ~40,000 t in 1992 (Ma et al., 2012) and increased to ~70,000 t in early 2000s (Wit et al., 2010). Rapidly increasing levels of PBDEs have been detected in the global environment, human, and other biota (Wang et al., 2006; Hites, 2004; Hardy, 2002). Due to high resistance to degradation, PBDEs can be bioaccumulated through food stuffs or exposure to PBDEs in the environment (Sjodin et al., 2003). Investigations show that PBDEs have a lot of adverse effects, including thyroid hormone disruption, permanent learning and memory impairment, behavioral changes, hearing deficits, delayed puberty onset, decreased sperm count, and fetal malformations in laboratory animals Hardy, 2002; Stoker et al., 2005; Viberg et al., 2006; Zhou et al., 2002; Branchi et al., 2003). Two major congeners of Penta-BDE, i.e., BDEs 47 and 99 (numbering is according to the IUPAC nomenclature for PCBs), show higher bioaccumulation factors than other PCBs of similar hydrophobicity. the production of penta- and octa-BDE mixtures was therefore phased out voluntarily by the manufacturers in the early 2000s and eventually ceased in the U.S. by the end of 2004 (Nouira et al., 2013).

Current analytical methods for PBDEs include GC/MS (Cochran and Frame, 1999; Akutsu et al., 2001; Cunha et al., 2010), gas chromatography (GC) (Sjodin et al., 1998), and high performance liquid chromatography–mass spectrometry (HPLC/MS) (Schlummer et al., 2005). Although good sensitivity has been achieved, these methods are somewhat expensive to operate, require complicated sample pretreatment processes (purification, concentration and/or derivatization), and are not suitable for in situ rapid analysis. Alternatively, immunoassay demonstrates high performances in fast analysis of vast samples due to its low cost and high specificity (Zhang et al., 2007; Zhao et al., 2011). Immunoassay of pentachlorophenol (PCP) (Kang et al., 2010) and octachlorostyrene (OCS) (Cai et al., 2013) were reported. In order to develop the immunoassay method of PBDE, BDE-121 (Fig. S1) has been chosen

* Corresponding author.
E-mail addresses: qycai0001@hnu.cn, caigroup@126.com (Q. Cai).

http://dx.doi.org/10.1016/j.bios.2014.04.058
0956-5663/

as a model compound of PBDE to develop its antibody in our group with an IC_{50} value of 8.07 ng mL^{-1} (Feng et al., 2014).

Label-free PEC immunoassay, based on the direct antigen–antibody affinity without markers, is a newly developed rapid, low-cost and high-throughput biological assay (Kang et al., 2010; Cai et al., 2013; Zhao et al., 2012). A favorable photoactive material is the key to guarantee good performances of a PEC sensor. Macroporous ZnO nanostructure can be a good PEC substrate due to its high specific surface area and favorable biocompatibility (Pan et al., 2001; Chen et al., 2011). The critical challenge for ZnO photoelectrode is the efficient utilization of solar energy, especially the visible light. One strategy is the use of narrow band gap QDs which can generate multiple electron–hole pairs per photon to improve the efficiency of utilizing visible light (Murphy et al., 2006). In this paper, CdTe QDs and Mn–CdS QDs are prepared to construct a stepwise structure of band-edge levels as CdTe/Mn–CdS/ZnO. Meanwhile, ZnS was introduced into the interfaces as buffer layers to improve the photostability (Xu et al., 2012). The ZnS layer acted as a potential barrier like an insulating layer employed in the conventional metal–insulator–semiconductor solar cells, allowing the adjustment of the electric field and potential distribution in the interface between the electrodes and the electrolyte and suppressing the dark current, resulting in further increase in the photoresponse. A label-free PEC immunosensor was constructed by immobilizing anti-BDE-121 polyclonal antibody on the ZnS/CdTe/Mn–CdS/ZnS/ZnO photoelectrode. The specific immunoreaction between BDE-121 and antibody formed steric hindrances hindering the transport of reduced reagent to the surface of the photoelectrode leading to decrease in photocurrent.

2. Materials and methods

2.1. Chemicals and materials

Zinc nitrate hexahydrate ($Zn(NO_3)_2 \cdot 6H_2O$), SnO_2:F (FTO) conductive glass substrates, sodium citrate, thioglycollic acid (TGA), manganese acetate, Na_2TeO_3, $NaBH_4$, chitosan(CS), glutaraldehyde, Tween 20, $Cd(NO_3)_2$, Na_2S, and Na_2SO_3 of analytical reagent grade were purchased from commercial sources and used as supplied. Ovalbumin (OVA) and bovine serum albumin (BSA) were purchased from Sigma-Aldrich Company. Mixed paint is purchased from the market. BDE-121 (10 ng/μL) was purchased from J&K Company. Phosphate buffer solution (PBS) was prepared with $NaHPO_4$ and Na_2HPO_4. Washing buffer is a PBS solution containing 0.05% (v/v) of Tween 20 (PBST). The assay solution was pH 7.4 phosphate-buffered saline solution in which 0.05% Tween 20 was added to increase the solubility of the analytes. Twice distilled water was used throughout the experiments. All experiments, excluding those with special annotation, are conducted at room temperature.

2.2. Fabrication of ZnS/CdTe/Mn–CdS/ZnS/ZnO NS photoelectrode

The ZnO NS was electrodeposited onto FTO substrate in an aqueous electrolyte containing 0.05 M $Zn(NO_3)_2 \cdot 6H_2O$ and 0.1 M KCl in a standard three electrode system with FTO (10 Ω cm^{-2}, Nippon sheet glass) as the work electrode, a platinum sheet counter electrode, and a Ag/AgCl reference electrode at −1.0 V and 70 C for 30 min using an electrochemical workstation (CHI660C, Shanghai Chenhua Instrument Co. Ltd.) (Qiu et al., 2011) The as-synthesized ZnO NS was sintered at 450 °C for 30 min in air atmosphere to obtain porous structure.

Water-soluble TGA-capped CdTe QDs were synthesized according to our previously reported method (Sheng et al., 2013, Supplementary information). We used bifunctional linker molecules (HOOC–R–SH) with carboxylate and thiol functional groups to facilitate the binding of CdTe QDs to ZnO NS. The CdTe QDs were directly absorbed onto the ZnO NS by immersing the ZnO NS in a CdTe QD aqueous solution at 25 °C for 12 h. The obtained CdTe QDs were stable for more than 6 months when stored at 4 °C.

Mn–CdS QDs were deposited onto the CdTe/ZnO NS using the SILAR method, i.e. the CdTe/ZnO NS was successively soaked, 30 s for each step, in solution containing 0.0375 M $Mn(NO_3)_2$, 0.05 M $Cd(NO_3)_2$, and 0.05 M Na_2S aqueous solutions, then rinsed with twice distilled water (Santra and Kamat, 2012). The TGA, absorbed onto the CdTe QD and ZnO NS, can capture Cd^{2+} to form CdTe/Mn–CdS core/shell QDs (Chuang et al., 2011). 9 SILAR cycles achieved the maximum photoelectric response (Fig. S13). For ZnS pre-treatment, 0.05 M $Zn(NO_3)_2$ in ethanol and 0.05 M Na_2S in methanol/water (7:3, v/v) were used for one SILAR process with a dipping time of 1 min for each cycle and repeated for 15 cycles. For ZnS post-treatment, dipping the sensitized photoelectrode two times in 0.1 M $Zn(NO_3)_2$ and 0.1 M Na_2S aqueous solutions for 1 min for each dipping (Xu et al., 2012; Lee et al., 2010).

2.3. Antibody preparation and immunosensor construction

The design and synthesis of hapten are critical to the immunoassay. A suitable hapten should preserve the structure of the target compound as much as possible. The synthesis of the BDE-121 hapten and the details of immunization procedures following the protocol described previously (Brun et al., 2008) are shown in Supplementary information (Figs. S2–S4). The developed BDE-121 polyclonal antibody serum shows a valence of 1:8000, inhibition of 8.07 ng mL^{-1}, and a linear range of 1.74–84.1 ng mL^{-1} (Fig. S11).

Scheme 1 shows the fabrication process of the immunosensor. 30 μL CS solution (0.05 wt% in 1% acetic acid) was daubed on a photoelectrode (3.0 cm^2) and dried at 50 °C. After washing with 0.01 M NaOH and water, the photoelectrode was immersed in 0.01 M PBS solution (pH=7.4) containing 5.0% glutaraldehyde at room temperature for 30 min, rinsed with water to remove the physically adsorbed glutaraldehyde, then immersed in 0.01 M PBS (pH=7.4) containing 0.5 mg mL^{-1} BDE-121 antibody at 37 °C for 12 h, and finally rinsed with PBST. The un-bonded sites were blocked by immersing the sensor in 0.01 M phosphate buffer (pH=7.4) containing 1% (w/v) OVA for 2 h at room temperature. The as-prepared sensor was washed with PBST thoroughly.

2.4. Photoelectrochemical measurements

All electrochemical measurements were performed with a CHI electrochemical analyzer (CHI660C, Shanghai Chenhua Instrument Co. Ltd.). The PEC activity of the photoelectrode was measured in 0.35 M Na_2SO_3 electrolyte containing 0.24 M Na_2S. The sensor was first immersed in BDE-121 solution in 5% dimethyl sulfoxide for 1 h at 37 °C (Fig. S12), then the PEC intensity of the sensor was detected in a 0.1 M pH 7.4 PBS solution containing 0.01 M Na_2S and 0.015 M Na_2SO_3 as the function of BDE-121 concentration.

3. Results and discussion

3.1. Photoelectrochemical behavior of the co-sensitized photoelectrode

The prepared ZnO NS showed sheetlike and three-dimensional hexagonal morphology (Fig. S5). Crystallization of the ZnO NS under 450 °C for 30 min turns the smooth surface (Fig. S5A) into a macroporous structure (Fig. S5C) probably due to the pyrolysis of

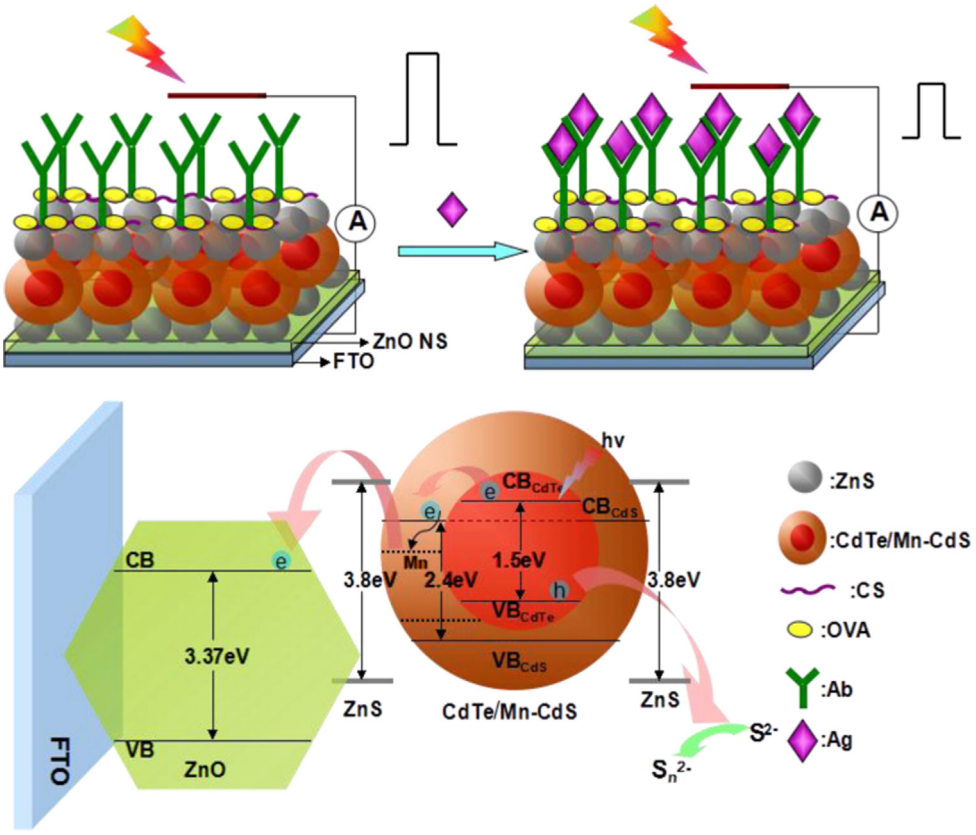

Scheme 1. Schematic diagram of the immunosensor construction process and the band diagram of the photoelectrode.

$Zn_5(OH)_8Cl_2 \cdot H_2O$:

$$Zn_5(OH)_8Cl_2 \cdot H_2O \rightarrow 5ZnO + 4H_2O\uparrow + 2HCl\uparrow$$

According to Qiu et al. (2011), the nanodeposits should be a mixture of ZnO and $Zn_5(OH)_8Cl_2 \cdot H_2O$.

The BET surface area of the hierarchically macroporous ZnO nanostructure was calculated to be 17.8 $m^2\,g^{-1}$, much bigger than that of ZnO powder ($<3\ m^2\,g^{-1}$) with similar size (Xu et al., 2007). The large specific surface area is mainly due to the macroporous structure embedded in three-dimensional micro-architectures. Such a structure is good for the following deposition of QDs. The TEM (JEOL, Japan) image of Fig. S5B_2 shows the spherical morphology of CdTe QDs in sizes ranging from 1 to 4 nm with an average size of 2.4 nm in diameter. Such sizes of CdTe QDs show the maximum photocurrent response according to our previous report (Sheng et al. 2013).

Modification of CdTe QDs with CdS QDs form core/shell CdTe/CdS QDs (Fig. S5B_3), ZnO NS was sufficiently covered with CdTe/CdS QDs (Fig. S5B_1) benefiting the carrier transport without space barriers. The deposition of the sensitizers does not obviously change the three-dimensional, macroporous morphology of ZnO NS, which will benefit the following PEC immunoassay for adsorption of the target molecule. HRTEM analysis of the CdTe/CdS/ZnO NS composite (Fig. S5D) clearly depicts that the crystallites connecting to the ZnO NS are CdTe are surrounded by CdS (Fig. S5D). CdS QDs with a polycrystalline structure are in close contact with both the CdTe QDs and ZnO NS, forming a cascade structure of CdTe/CdS assembled in the ZnO NS. The EDS spectrum (Fig. S5B_1) exhibits the characteristic peaks of Cd, Te, S, Zn, and O; the Te peak is very weak, with an elemental analysis corresponding to 0.30 at% of the film. The details of the characterization is shown in Supplementary information

The performances of a photoelectrode depend on the abilities of adsorption of light and the separation of photogenerated electrons/holes. The recombination rate of electrons/holes can be characterized with fluorescence intensity (Hitachi, Japan); a lower fluorescence intensity suggests a lower recombination rate. CdTe QDs show an emission peak at 554nm while on clean FTO substrate (Fig. S6). When CdTe QDs are anchored onto ZnO NS, the emission at 554 nm is significant quenched (curve b). Further coating the CdTe/ZnO photoelectrode with CdS QDs or Mn–CdS QDs, the emission at 554 nm is further quenched (curves d and e), indicating that the recombination of electrons/holes is reduced with modifications of sensitizers. The naked ZnO NS films absorb only UV light (Cary 300, USA). After sensitization, the absorption edge of the ZnO NS films extends to the visible light region. The absorption edges of CdS/ZnO NS and CdTe/ZnO NS have redshifts corresponding to band gaps of 2.4 eV and 1.5 eV, respectively. Subsequent growth of CdS QDs or Mn–CdS QDs on CdTe QDs results in signficant enhancement in the light absorption in the visible light region (inset Fig. S6).

The good absorption properties of the CdTe/Mn–CdS-sensitized photoelectrode were demonstrated in photocurrent. The core–shell CdTe/CdS/ZnO photoelectrode demonstrated a photocurrent density of as high as $\sim$4.06 mA cm^{-2} (Fig. S7), dramatically higher than that obtained with CdS QDs (1.71 mA cm^{-2}) or CdTe QDs (0.77 mA cm^{-2})-coated electrodes (Fig. S13). The higher short-circuit current density (J_{sc}) of the CdS QDs sensitized photoelectrode is attributed to its broader light absorption range compared with that of the CdTe QDs-sensitized ZnO NS photoelectrodes (Fig. S6). For the core/shell CdTe/CdS/ZnO NS photoelectrode, the photocurrent density increased to $\approx$4.06 mA cm^{-2}, dramatically larger than the values obtained with only individual CdS QDs or CdTe QDs. A type II-like core/shell model is proposed to elucidate the possible charge transfer mechanism in CdTe/CdS co-sensitized

photoelectrode system. In an ideal type II core–shell QD, the spatially separated electron and hole wave functions reduced their coulomb interaction, increasing the lifetimes of single and multiple exciton states. Meanwhile, shell-localized electrons and core localized holes could achieve ultrafast electron transfer to adsorbed acceptors while simultaneously retarding the charge recombination process (Zhu et al., 2011). Further coating of Mn–CdS QDs resulted in a 21% increase in the photocurrent (4.9 mA cm^{-2}) Comparing these photocurrent results, one can see that besides the contributions of these individual sensitizers to photocurrent, other factors play a leading role in the enhancement of photocurrent, which is assigned as a stepwise band-edge level, namely the type-II structure in the core/shell CdTe/Mn–CdS sensitized photoelectrode (Scheme 1) (Luo et al., 2013; Song et al., 2010). ZnS buffer layers within interfaces were used to passivate the surface states of ZnO NS and block the ZnO surface, suppressing the recombination of electrons/holes at the interfaces. The ZnS post-treatment layer acted as a potential barrier to adjust the electric field and potential distribution in interface, suppressing the dark current (Xu et al., 2012; Lee et al., 2010), leading to the photocurrent enhanced to 6.23 mA cm^{-2}. Under AM 1.5 G illumination, the correspondent photoelectrochemical cell efficiency is 4.20% which is among the highest reported to date for ZnO NS based photoelectrodes (Fig. S14). Continuous illumination of 30 min resulted in 0.8% decrease in photocurrent, indicating an excellent photostability of the ZnS/CdTe/Mn–CdS/ZnS/ZnO photoelectrode (Fig. S7).

3.2. Performances of the PEC immunosensor

A BDE-121 PEC biosensor was fabricated by modifying the co-sensitized photoelectrode with anti-BDE-121 antibody. The corresponding photocurrent variations induced by modification progress are shown in Fig. S8. The successive immobilizations of anti-BDE-121 and OVA result in continuous decrease in photocurrent intensity (Fig. S8, curves b and c) due to the increase in steric hindrances. The specific immunoreaction between BDE-121 and the anti-BDE-121 antibody forms an immunocomplex leading to further decrease in photocurrent (Fig. S8, curve e). In order to confirm that the decrease in photocurrent resulted from the immunoreaction, a blank experiment was conducted. The immunosensor was incubated with 5% dimethyl sulfoxide solution without BDE-121 at 37 °C for 1 h, then the photocurrent was measured. There is no apparent change in photocurrent intensity (Fig. S8, curve d). As an effective tool to characterize the interface properties of the photoelectrode, electrochemical impedance spectroscopy (EIS) was also utilized to monitor the fabrication process. The incubation of the immunosensor in BDE-121 solution results in further decrease in the resistance (Fig. S9, curve e) due to the formation of an immunocomplex.

BDE-121 was quantified based on the BDE-121-resulted decreases in photocurrent. As a mild pH solution was required in biosensing, the detection was conducted in a pH = 7.4 PBS solution (0.1 M) containing 0.01 M Na_2S and 0.015 M Na_2SO_3, typical oxidative quenchers in photoelectrochemical cell (Chakrapani et al., 2011). The consumption of holes benefits the separation of electrons and holes, leading to an increase in photocurrent. Fig. 1 displays typical photocurrent responses of the biosensor to different concentrations of BDE-121 for 1000 nM, 500 nM, 100 nM, 50 nM, 10 nM, 5 nM, 1 nM, 0.5 nM, 0.1 nM, 0.05 nM, 0.01 nM, 0.005 nM, 0.0025 nM, and 0.001 nM. Basically, it is impossible to make every PEC biosensor completely the same even in a same batch. As the sensor-to-sensor differences exist, it is necessary to find an internal reference to calibrate the responses. In the present work, the blank response without BDE-121 was used as the internal reference. The decrease in photocurrent is dependent on the BDE-121 concentration as Fig. 1A. The corresponding photocurrent–time response with concentration range from 1000 nM to 0.001 nM (curves a–n) obtained on three different PEC biosensors were normalized with the blank response and shown in inset of Fig. 1A. One can see that the sensor-to-sensor difference is basically eliminated. Due to limited sensitivity and amounts of capture molecules (antibody) of the sensor, there is almost no photocurrent change at lowest and highest concentration levels, i.e., for curve (a) and (b), curve (m) and (n). Correspondingly, as shown in Fig. 1B and the inset (entire concentration range), the photocurrent decrement was linearly proportional to the logarithmic value of the BDE-121 concentration in the range of 0.005 nM to 100 nM with a correlation coefficient of 0.9993, and a regression equation of:

$$(I_0 - I)/I_0 = 1.5582 + 0.1266 \log C$$

where I_0, I are the photocurrents of the biosensor before and after reaction with BDE-121, respectively, and C the concentration of BDE-121. Here, more BDE-121 was immobilized on the biosensor with increasing concentrations, leading to decreased photocurrent intensity (I). So, photocurrent response ($(I_0 - I)/I_0$) gradually increases with increasing logarithm of BDE-121 concentrations.

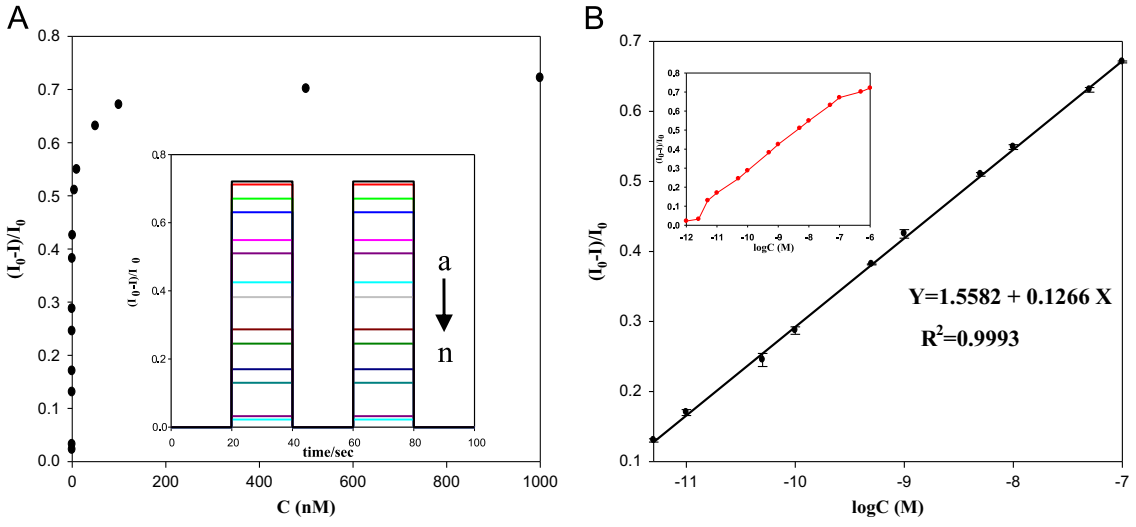

Fig. 1. (A) Photocurrent responses of immunosensor in the presence of various BDE-121 from 1 pM to 1 μM upon light on/off, and (B) the corresponding calibration curve (R^2 = 0.9993).

We have added the contrast test to confirm the high capacity for target analytes of the macroporous ZnO NS. If the co-sensitized photoelectrode is prepared with smooth ZnO NS (without crystallization), the limit of detection for BDE-121 assay is only 50 nM, demonstrating a superior singal amplification ability of the macroporous nanostructure. The calculated detection limit corresponding to the response of three times the standard deviation of zero-dose response ($n=10$) is 3.98 pM, which is much lower than those published values, such as ELISA (0.644 ng mL^{-1}) (Feng et al., 2014), and HPLC–UV/MS (10 ng mL^{-1}) (Schlummer et al., 2005).

The reproducibility of an assay was expressed in terms of relative standard deviation (RSD) determined in a within-batch (intra-assay) and a between-batch (interassay). The determination of 1×10^{-8} M BDE-121 solution five times gave an intra-assay RSD of 5.9%. The interassay RSD on seven immunosensors is 6.5%. The results show good precision and acceptable fabrication reproducibility. When the immunosensor was stored in a dry condition at 4 °C for a week, over 90% of the initial response remained, indicating acceptable reliability and stability.

Fig. 2A shows responses toward 1×10^{-8} M BDE-121 and benzene series interferences with concentrations of 50-fold that of BDE-121; the interferences of these compounds are little, indicating a high specificity of the proposed biosensor. The achieved sensitivity, specificity, and stability guarantee of the sensor can be applied to measure BDE-121 in real paint samples.

3.3. Analysis of furniture foam and paint samples

In order to ascertain the potential applications of the sensor, furniture foam and paint samples were analyzed with the sensor. Fig. 2B shows the analytical results of the samples with both the GC/MS (Thermo Finnigan, USA) and the proposed biosensor. The samples were extracted by addition of 3×10 mL n-hexane/dichloromethane ($V/V=1:1$) into 10 g paint sample or 1 g furniture foam sample. After stirring for 24 h, the organic phase was filtered with filter paper and 0.22 μm cellulose membranes, and collected. After drying with a rotary evaporator, 300 μL n-hexane/dichloromethane was added to the residual. 200 μL of the organic solution was directly analyzed by GC/MS giving a content of 1.16 ng mL^{-1} based on the peak area of known BDE-121 samples (Fig. S10). In order to cover the wide linear detection range of the proposed protocol, 100 μL of the residual solution was dried and used either as-received or diluted to a specific concentration including 0.016, 0.16, 1.16 ng mL^{-1} with 5% dimethyl sulfoxide for PEC immunoassay. The paint samples had the highest recovery rate ranging from 105% to 114%. The BDE-121 content is calculated to be 1.32 ± 0.02 ng mL^{-1}. The BDE-121 content measured by the PEC sensor is higher than that obtained by GC/MS. It is likely that interferents existing in paint sample lead to a positive deviation. From Fig. 2B one can see that the paint sample has complicated compositions. The sensitive responses of these compounds on GC/MS indicate that some of them are organic halides which would have responses in the PEC sensor. For a fast and simple method, this result is acceptable. As shown in Fig. 2B (right), BDE-121 was not detected in the furniture foam sample due to the low concentration. So the furniture foam samples spiked with BDE-121 at concentrations of 0.028, 0.28 and 2.8 ng mL^{-1} were treated in the same way for recovery investigation, The recovery of all the measured samples is between 94% and 98% indicating that the possible interference from sample media is negligible. All the measured results are summarized in Table S1.

4. Conclusions

ZnS/CdTe/Mn–CdS/ZnS/ZnO NS photoelectrode was successfully prepared and applied as the substrate of a BDE-121 PEC immunosensor. The three-dimensional, macroporous ZnO NS contributes a high loading of sensitizer and high capacity of the target analytes for use in PEC immunoassay, leading to high responses. The photocurrent intensity of the ZnO NS is greatly enhanced by co-sensitization with CdTe and Mn–CdS QDs, the essence of this property is the formation of a core–shell stepwise band-edge structure which is advantageous to the transport of excited electrons and holes across the composite. Introduction of ZnS into the CdTe/Mn–CdS/ZnO NS greatly enhanced the photostability. The label-free PEC immunosensor shows high sensitivity and specificity to BDE-121. The analysis of BDE-121 in paint sample illustrated the applicability of the immunosensor. In the present work, the change in photocurrent resulted from the formation of antibody-BDE-121 immunocomplexes. So, for analysis of large targets, the proposed PEC platform will be more suitable.

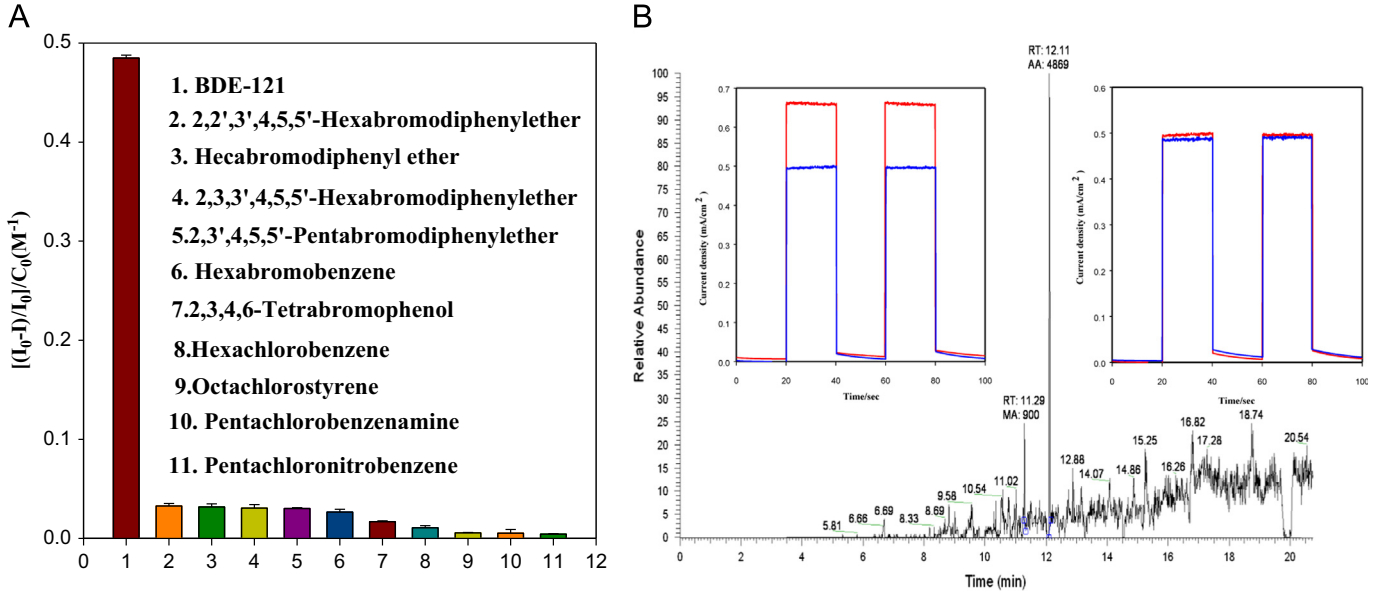

Fig. 2. (A) The interfering effects of other related benzene series on the PEC signal of the immunoassay and (B) GC–MS analysis of the paint sample. The inset shows the photocurrent response of the sensor, furniture foam (right) and paint sample (left).

Acknowledgment

This work was financially supported by the National Basic Research Program of China (Grant no. 2009CB421601), and the National Natural Science Foundation of China (Grant no. 21175038 and 21235002).

Appendix A. Supporting information

Supplementary data associated with this article can be found in the online version at http://dx.doi.org/10.1016/j.bios.2014.04.058.

References

Akutsu, K., Obana, H., Okihashi, M., Kitagawa, M., Nakazawa, H., Matsuki, Y., Makino, T., Oda, H., Hori, S., 2001. Chemosphere 44, 1325–1333.
Branchi, I., Capone, F., Alleva, E., Costa, L.G., 2003. Neurotoxicology 24, 449–462.
Brun, E.M., Bonet, E., Puchades, R., Maquieira, Á., 2008. Environ. Sci. Technol. 42, 1665–1672.
Cai, J., Sheng, P.T., Zhou, L.P., Shi, L., Wang, N.Y., Cai, Q.Y., 2013. Biosens. Bioelectron. 50, 66–71.
Chakrapani, V., Baker, D., Kamat, P.V., 2011. J. Am. Chem. Soc. 133, 9607–9615.
Chen, H.N., Li, W.P., Liu, H.C., Zhu, L.Q., 2011. Electrochem. Commun. 13, 331–334.
Chuang, C.H., Doane, T.L., Lo, S.S., Scholes, G.D., Burda, C., 2011. ACS Nano 5, 6016–6024.
Cochran, J.W., Frame, G.M., 1999. J. Chromatogr. A 843, 323–368.
Cunha, S.C., Kalachova, K., Pulkrabova, J., Fernandes, J.O., Oliveira, M.B.P.P., Alves, A., 2010. Chemosphere 78, 1263–1271.
Feng, H.Y., Zhou, L.P., Shi, L., Li, W.L., Yuan, L.J., Li, D.Q., Cai, Q.Y., 2014. Anal. Biochem. 447, 49–54.
Hardy, M.L., 2002. Chemosphere 46, 757–777.
Hites, R.A., 2004. Environ. Sci. Technol. 38, 945–956.
Kang, Q., Yang, L., Chen, Y., Luo, S., Wen, L., Cai, Q., Yao, S., 2010. Anal. Chem. 82, 9749–9754.
Lee, H., Bang, J., Park, J., Kim, S., Park, S., 2010. Chem. Mater. 22, 5636–5643.
Luo, J.H., Wei, H.Y., Huang, Q.L., Hu, X., Zhao, H.F., Yu, R.C., Li, D.M., Luo, Y.H., Meng, Q.B., 2013. Chem. Commun. 49, 3881–3883.
Ma, J., Qiu, X., Zhang, J., Duan, X., Zhu, T., 2012. Chemosphere 88, 769–778.
Murphy, J.E., Beard, M.C., Norman, A.G., Ahrenkiel, S.P., Johnson, J.C., Yu, P.R., Mićić, O.I., Ellingson, R.J., Nozik, A.J., 2006. J. Am. Chem. Soc. 128, 3241–3247.
Nouira, T., Risso, C., Lassaad, C., Budzinski, H., Boussetta, H., 2013. Chemosphere 93, 487–493.
Pan, Z.W., Dai, Z.R., Wang, Z.L., 2001. Science 291, 1947–1949.
Qiu, J.H., Guo, M., Wang, X.D., 2011. Appl. Mater. Interfaces 3, 2358–2367.
Santra, P.K., Kamat, P.V., 2012. J. Am. Chem. Soc. 134, 2508–2511.
Schlummer, M., Brandl, F., Mäurer, A., Eldik, R. van., 2005. J. Chromatogr. A 1064, 39–51.
Sheng, P.T., Li, W.L., Cai, J., Wang, X., Tong, X., Cai, Q.Y., Grimes, C.A., 2013. J. Mater. Chem. A 1, 7806–7815.
Sjodin, A., Jakobsson, E., Kierkegaard, A., Marsh, G., Sellstrom, U., 1998. J. Chromatogr. A 22, 83–89.
Sjodin, A., Patterson Jr, D.G., Bergman, A., 2003. Environ. Int. 29, 829–839.
Song, X., Fu, Y.S., Xie, Y., Song, J.G., Wang, H.L., Sun, J., Du, X.W., 2010. Semicond. Sci. Technol. 25, 045031.
Stoker, T.E., Cooper, R.L., Lambright, C.S., Wilson, V.S., Furr, J., Gray, L.E., 2005. Toxicol. Appl. Pharmacol. 207, 78–88.
Viberg, H., Johansson, N., Fredriksson, A., Eriksson, J., Marsh, G., Eriksson, P., 2006. Toxicol. Sci. 92, 211–218.
Wang, J.X., Jiang, D.Q., Gu, Z.Y., Yan, X.P., 2006. J. Chromatogr. A 1137, 8–14.
Wit, C.A.d., Herzke, D., Vorkamp, K., 2010. Sci. Total Environ. 408, 2885–2918.
Xu, F., Zhang, P., Navrotsky, A., Yuan, Z.Y., Ren, T.Z., Halasa, M., Su, B.L., 2007. Chem. Mater. 19, 5680–5686.
Xu, G.P., Ji, S.L., Miao, C.H., Liu, G.D., Ye, C.H., 2012. J. Mater. Chem. 22, 4890–4896.
Yang, M., Qi, H., Jia, H.L., Ren, N.Q., Ding, Y.S., Ma, W.L., Liu, L.Y., Hayley, H., Ed, S., Li, Y.F., 2013. Environ. Sci. Technol. 47, 8978–8984.
Zhang, S.B., Wu, Z.S., Guo, M.M., Shen, G.L., Yu, R.Q., 2007. Talanta 71, 1530–1535.
Zhao, W.W., Ma, Z.Y., Yu, P.P., Dong, X.Y., Xu, J.J., Chen, H.Y., 2011. Anal. Chem. 84, 917–923.
Zhao, W.W., Ma, Z.Y., Yan, D.Y., Xu, J.J., Chen, H.Y., 2012. Anal. Chem. 84, 10518–10521.
Zhou, T., Taylor, M.M., DeVito, M.J., Crofton, K.M., 2002. Toxicol. Sci. 66, 105–116.
Zhu, H.M., Song, N.H., Lian, T.Q., 2011. J. Am. Chem. Soc. 133, 8762–8771.